2014

Heat Transfer Enhancement by Three-Dimensional Surface Roughness Technique in Nuclear Fuel Rod Bundles

Kang Liu
University of South Carolina - Columbia

HEAT TRANSFER ENHANCEMENT BY THREE-DIMENSIONAL SURFACE ROUGHNESS TECHNIQUE IN NUCLEAR FUEL ROD BUNDLES

By

Kang Liu

Bachelor of Science

University of Science and Technology of China, 2008

Submitted in Partial Fulfillment of the Requirements

For the Degree of Master of Science in

Mechanical Engineering

College of Engineering and Computing

University of South Carolina

2013

Accepted by:

Jamil A. Khan, Director of Thesis

Chen Li , Reader

Lacy Ford, Vice Provost and Dean of Graduate Studies

ACKNOWLEDGEMENTS

This dissertation would not have been possible without the guidance and the help of several individuals who in one way or another contributed and extended their valuable assistance in the preparation and completion of this study.

First and foremost, my utmost gratitude to Dr. Jamil Khan, Chair of the mechanical engineering department of University of South Carolina Columbia, whose kindness and encouragement I will never forget. Dr. Khan has been my inspiration as I hurdle all the obstacles in the completion of this research work.

Secondly the author would like to thank Prof. Chen Li for being his committee member and valuable advice on thesis.

Thirdly the author would like to thank all his colleagues in the thermal research group, Mr Umair Najeeb, Mr. Titan Paul, Dr. Ruixian Fang and Dr. Monjur Morshed for their invaluable suggestions, comments and help.

Above all I would like to thank Westinghouse Electric Company, Columbia, SC for funding the project. Specifically I would like to thank Dr. Zeses Karoutas for providing technical and financial support and Dr. Leo Carrilho for designing the experimental facility.

At last the author would like to dedicate this dissertation to his families for their continuous support, understanding and care.

ABSTRACT

This thesis investigate the thermal characteristic of a single-phase nano-fluid in a single heater element loop tester and provides a comparison between heat transfer enhancement results achieved using water as a coolant and using nano-fluids with different volume percentage. The experimental investigation is performed on two simulated nuclear fuel rods with two different types of modified outer surfaces roughness. The fuel rod surfaces modified are termed as two-dimensional surface roughness (square transverse ribbed surface) and three-dimensional surface roughness (Diamond shaped blocks). The nano-fluid used are 0.5% and 2% ZnO-Deionized water based nano-fluid. The maximum heat transfer co-efficient enhancement achieved compared to DI-water was **33%** at **Re=1.15e5** for fuel rod with three-dimensional surface roughness using **2%** (volumetric concentration) **ZnO** nano-fluid. It was also observed that the increase in **Re** number results in higher heat transfer co-efficient. It's concluded in this report that the Nano-fluids give a better thermal performance than the deionized (DI) water and diamond shape roughness devotes higher heat transfer coefficient than helically ribbed surface roughness using nano-fluid. A substantial amount of nano-particle deposition was observed on the fuel rod surface when the experiments were performed at higher bulk fluid temperature. The nano-particle deposition layer created hot spots along the rod surface resulting in inconsistent heat transfer in the fuel rod bundle. Therefore experiments were suspended at higher temperatures.

TABLE OF CONTENTS

LIST OF TABLES

LIST OF FIGURES

LIST OF SYMBOLS

A_h Hydraulic area of annulus test section, m^2

C_p Specific heat, kJ/kg-K

D_h Hydraulic diameter, mm

d_0 Outer diameter of heater rod, mm

d_i Inner diameter of heater rod, mm

D_i Inner diameter of test section, mm

h Heat transfer coefficient, $W/m^{2-}K$

I Current, Amps

k_f Thermal conductivity of water, W/m-K

l Length of heater rod, inch

$\dot{m}$ Mass flow rate, kg/s

Nu Nusselt number

P Power, Watt

$\dot{Q}$ Volumetric flow rate, m^3/ hr

Q Heat transfer rate, Watt

Q'' Heat flux, Watt/m^2

Greek Symbols:

Q'''	Rate of heat generation, Watt/m^3
Re	Reynolds number
Re_D	Test Section Reynolds number
T	Temperature, ^oC
T_b	Bulk fluid temperature, ^oC
T_i	fluid temperature at test-section inlet, ^oC
T_m	mean fluid temperature, ^oC
$T_{s,i}$	Heater rod inner surface temperature, ^oC
$T_{s,o}$	Heater rod outer surface temperature, ^oC
T_w	Wall Temperature, ^oC
T_o	Fluid temperature at test-section outlet, ^oC
v	Fluid velocity, m/s
V	Input voltage, volt
μ	Dynamic viscosity
ρ	Fluid density

Subscripts:

f	Fluid
i	Inlet
o	Outlet
r	Rough section

s	Smooth section
enh	Enhancement

CHAPTER 1

INTRODUCTION

As the global need for energy is growing at an exponential rate, more and more power plants are being built year after year. One of the key challenges in all energy generation processes is the need for efficient heat removal, this need is more pronounced in nuclear rod bundles of power reactors. An efficient and high heat flux from the rod-bundles to the coolant allows for the center of the rods to be not heated. This results in more efficient power production. Though many traditional heat transfer augmentation method is being adopted, new and more effective ways are being searched and explored by the scientists.

1.1 Heat transfer Enhancement Techniques

It's not so late now before we realize the insufficiency of the energy in the world, as a result of this, energy-efficiency is becoming more important than ever. Heat transfer has a dominant role in improving the efficiency of the thermal systems. Therefore we have to advance the techniques to enhance the heat transfer rate, specifically by increasing of the heat transfer coefficient from the same input.

Much research has been done on this field and still many research groups are allocating huge resources on developing cutting-edge techniques to obtain higher heat transfer rate in thermal systems. In general, the techniques for single phase heat transfer enhancement are classified as: **Active techniques and Passive techniques**. These heat transfer enhancement techniques can various enhancement factors, such as, boundary

layer breakup, flow transition, entrance region effect, vibration, secondary flow, swirl flow, electrical fields and mixtures etc. for increasing the heat transfer rates.

Active techniques usually involves external inputs, for instance, electrical power or RF signals are commonly used causing flow pulsation, vibration, synthetic-jet etc.

The passive techniques can normally be seen as flow disruption, secondary flow, entrance effects, introduction of nano-fluid or surface treatments, etc. In this current study we focus on **surface treatment** and **nano-fluid**. The conventional way of surface treatment is to make it rough so that the appearance of the turbulence could help to enhance the heat transfer coefficient. Nano-fluid method is to use of ultra-fine nano particles to increase the thermal conductivity of the base fluid as well as heat transfer properties. These ultra-fine nano-particles can be mixed with base fluid such as water, ethylene-glycol and engine oil to form composite nano-fluids. The normal concentration range of nano-particles in a base fluid used for enhancement of heat transfer varies from 0.1% to 5% by volume.

1.2 Heat transfer enhancement in annular spaces and structure

As is well known, turbulence can significantly increase the heat transfer rate. In figure 1.1, we can see the currently practiced enhancement of the heat transfer technique in a PWR Nuclear Fuel Rod Bundle. Here, the structural grids are orderly located with vanes.

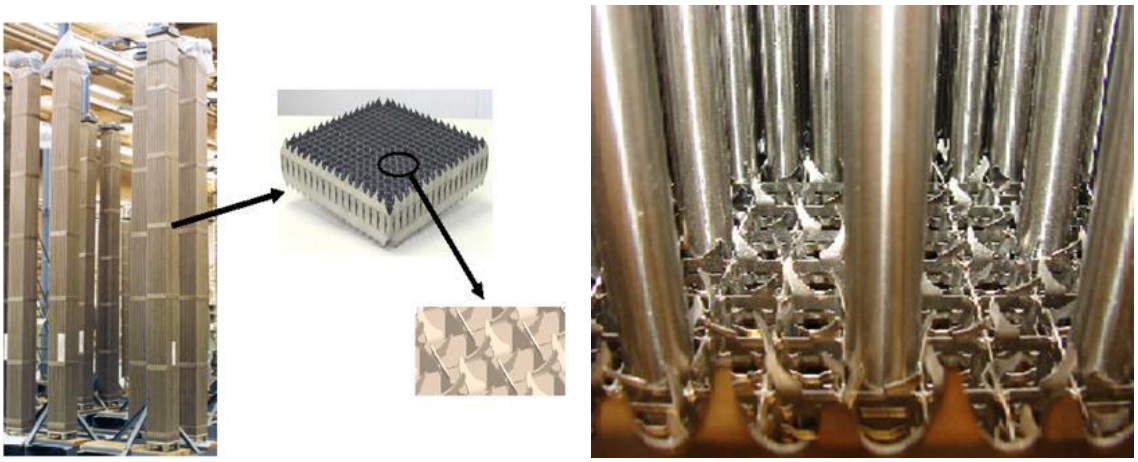

Figure 1.1 PWR Rod Bundle / Structural Grid /Mixing Vanes

At high speed of flow with higher pressure, when reached limit, the vane would chip off triggering irregular turbulence along the rod span, enhancing flow mixing and heat transfer rate. Unfortunately the distribution of the turbulence along the rod span is not uniform, and heat transfer rate is localized near the structural grid, as the flow moves further from the vanes, the weaker the turbulence fades which causes the heat transfer to decrease dramatically.

1.3 Thesis Proposal

Previous research work by Umair Najeeb (2012) was focused on heat transfer enhancement by using surface treatment to investigate its effects on the heat transfer of the coolant and the resulting pressure drop across the fuel rod in a close loop simulating a single rod of nuclear rod bundle. In his research he studied a diamond shaped, three dimensional roughness introduced on the rod. He compared the resulting enhanced heat transfer coefficient and friction factor ibn the rough section with that of the smooth section using deionized water as the coolant.

With the use of three dimensional roughness, we obtained promising results in enhancing heat transfer coefficient. Heat transfer enhancement of greater than 80 percent

has been achieved at Re=4.18E+05. It was also observed that the pressure drop and friction factor increased only by 14.7% due to the surface roughness. The result encouraged us to find the possibility of further enhancement of heat transfer using alternate feasible methods, therefore we decided to study nano-fluid with lower specific heat capacity instead of DI-water. The proposed experimental facility was modified to eliminate any hot spots along the rod span and render uniform distribution of turbulence at the test section. We also propose the tests to be performed under different flow rates and various temperatures. Our objective is to compare the result of tests with 2-dimensional and 3-dimensional roughness with the nano-fluid as the coolants.

CHAPTER 2

LITERATURE REVIEW

2.1 Surface Roughness Technique

A significant amount of research on the surface roughness technique have been done by the scientists. At first, surface roughness technique belongs to passive techniques according to the research of A.E. Bergles, A.R. Blumenkrantz (1974). Furthermore, D.N Ryu, D.H. Choi, V.C Patel (2007) give the conclusion that the artificial surface roughness enhances the heat transfer by triggering the thermal layer breakup as well as facilitating intensive turbulent mixing. This phenomenon, however, is accompanied by unexpected raise of frictional resistance.

In Steinke and Kandlikar, (2004), the author concluded that for the single-phase fluid flow, classical theory still works. As mentioned earlier, the major heat transfer enhancement techniques for conventional channel include flow transition, breakup of boundary layer, entrance effect, vibration, electric fields, swirl flow, secondary flow and mixers, etc. However, due to the small size of micro-channel heat sinks, only a few of these techniques can be extended into micro-channel applications. Steinke and Kandlikar (2004) evaluated the possibilities of some of those techniques for single-phase flows in micro-channels.

2.2 Different Roughness

Surface roughness can be categorized respectively as One-dimensional (1D), Two-dimensional (2D) and Three-Dimensional (3D) surface roughness. One example of the one

dimensional roughness is creating rough surface in micro channels by growing 1D nano-structure like nano-wires on micro channel surface for heat transfer enhancement (Figure 2.1).

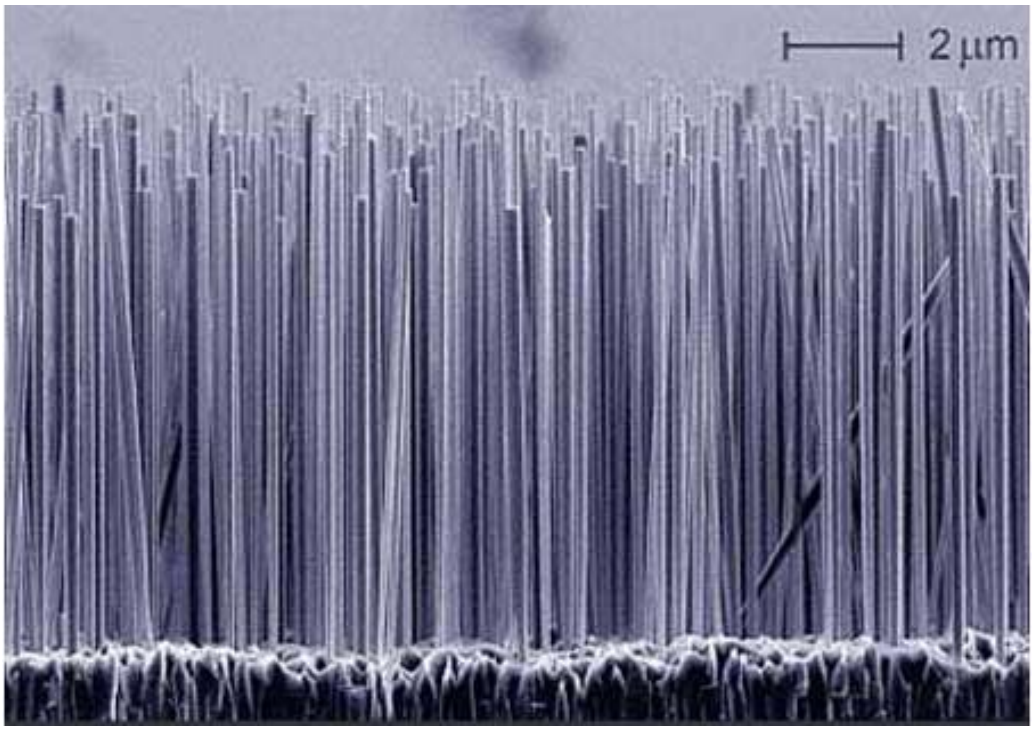

Figure 2.1: An array of silicon nanowires by Magnus Borgström (Jan. 23rd 2001)

The two-dimensional surface roughness are mainly used in conventional flow channels to enhance heat transfer by convection. There are four different types of 2-D roughness. Firth, R.J. and Meyer, L., (1983) conducted the research on heat transfer performance as well as friction factor of these four different types of artificially roughened surface. Three of these surfaces are Two-dimensional roughened surfaces. These surfaces are:

1. Square transverse ribbed surface (Figure 2.2)
2. Helically ribbed surface(Figure 2.3)
3. Trapezoidal transverse ribbed surface(Figure 2.4)

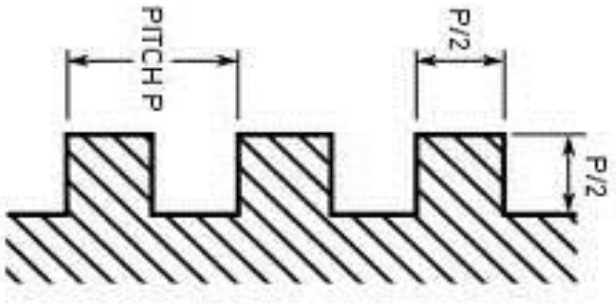

Figure 2.2: Square Transverse Ribbed Surface

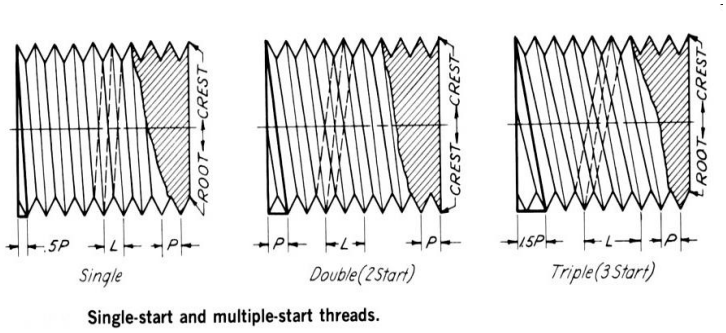

Figure 2.3: Helically Ribbed Surface

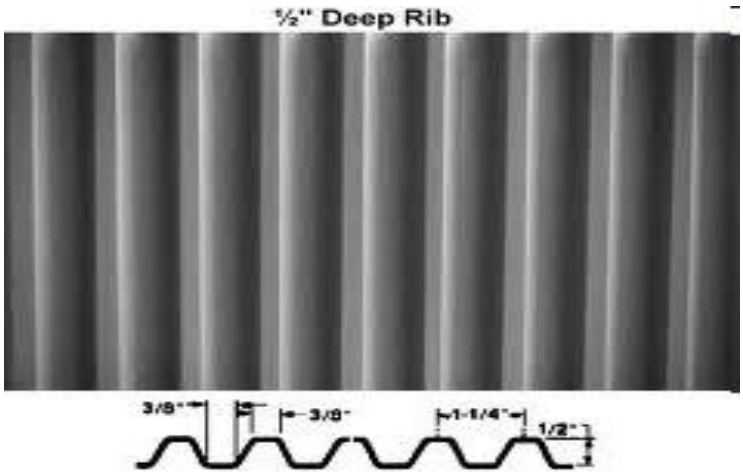

Figure 2.4: Trapezoidal Transverse Ribbed Surface

The roughened surfaces are intended to improve the speed of heat distraction from the fuel pins in the reactors which used gaseous coolant. All the tests were conducted under fully-developed and turbulent flow conditions with Reynolds's number up to $5x10^5$. The pin with the roughened surface was located at the center of a smooth outer channel and heated up electrically. The result showed that square transverse ribs had a higher friction factor than the trapezoidal transverse ribs as a result of higher rib height to width ratio and the more amount of rib rounding. Whereas, because of reduced angle of attack the helically ribbed surface had a lower friction factor. The key result was that enhancement in heat transfer is achieved at the expense of higher friction factor. Also the result showed that heat transfer was enhanced along the rough region by great amount. In the study the comparison of these roughness shows a relative thermal performance of these three surfaces, which revealed that trapezoidal transverse ribbed surface is the lowest among all these surfaces. The square transverse ribbed surface and helically ribbed surface have comparable levels of thermal performance.

Han and Park (1985) studied heat transfer performance of two oppositely rib-roughened walls and smooth walls in a rectangular channel. They determined the effects of rib pitch to height ratio, angle of attack, friction factor and heat transfer co-efficient in a fully developed flow. It could be concluded that Stanton number of roughened wall and heat transfer co-efficient were two to three times higher than those of the smooth wall. For the same experiment they used another rectangular and square test section and also studied the influence of different angle of attack and aspect ratio on local heat transfer co-efficient and friction factor. The study showed that in square channels, ribs at angle of attack of 60 degrees resulted in the most heat transfer and pressure drop through the rough region.

Similarly, the ribs at the angle of attack of 30 and 45 degrees resulted in best cooling. Singh, S. and Chander, S. (2011) conducted investigations on rectangular duct with one board wall roughened into discrete V-down rib under constant heat flux. The result showed Nusselt number and friction factor for roughened duct compared to smooth duct were enhanced by 51.4% and 26.5% respectively. The maximum enhancement of Nusselt number for roughened duct compared to smooth duct was found to be 3.04 while the max friction factor 3.11.

X. Li and J. Meng. (2011) conducted experiment on getting heat transfer co-efficient of two-dimensional roughness tubes with various roughness heights under different Reynolds numbers. They concluded that there is maximum Nusselt number and Reynolds number ratio for each roughness height. In the result they found that when the roughness height was more than five times of the viscous sub layer thickness, the flow friction began to increase greatly but the heat transfer was barely increasing. They had the conclusion that the most heat transfer enhancement at given power was when roughness height was three times of viscous sub layer thickness.

D.N Ryu , D.H. Choi , V.C Patel (2007) conducted an investigation to analyze the resistance in turbulent flow channels roughened by two-dimensional ribs(square ribs, triangular ribs, semicircular ribs, wavy wall) and three-dimensional blocks. Result showed that the square ribs contributed the most resistance among the four kinds of roughness whereas the wavy wall had the lowest. In the second part of their experiment they analyzed the heat transfer augmentation in turbulent flow channels respectively in all those kinds of roughened surface. They came to the conclusion that the geometry for maximum heat transfer, i-e., highest average Nusselt number, is co-related to that of maximum resistance

co-efficient for ribs. Generally speaking, the most heat enhancement is provided by the square rib, and heat transfer was not efficient as the shape changes to other textures.

Another heat transfer enhancement technique for surface treatment is the three-dimensional surface roughness. Artificially corrugated three-dimensional channels are often used in rotary regenerators and plate-type heat exchangers. Three-dimensional blocks are commonly used as three-dimensional surface roughness structure. These blocks can be like diamond-shaped, rectangular, parallelogram-shaped or hexagonal.

Ralph L. Webb and Nae-Hyun Kim (2005) conducted a series of experiment using the given corrugated channels specified by pitch, channel height wall thickness and angle of corrugation. Focke et al. (1985), Stasiek et al. (1996) investigated the effect of corrugation angle 'Θ' ranging from 0° to 90°. Result showed that as Θ increased, the friction factor increased considerably as well. Focke et al. (1985) also observed that swirl in furrows was produced as a result of the velocity component of the fluid moving along the opposite furrows in a direction perpendicular to the furrow and the maximum swirl can be achieved when Θ = 45°.

Figure 2.5: Three-dimensional Surface Roughness

Firth, R.J. and Meyer, L., (1983) investigated the heat transfer and friction factor performance of both 2-D (3 types)and 3-D artificially roughened surfaces. Their result showed that the trapezoidal transverse ribs had a lower friction factor than square transverse ribs due to the lower rib height to width ratio. The helically ribbed surface had lower friction factor than transverse ribs as a result of the reduced 'angle of attack'. Also the three-dimensional surface had the highest friction factor due to a higher density of effective leading surface. Another valuable result was that three-dimensional surface provided the best thermal performance, which had an improvement of over 15% compared with all the other kinds of two-dimensional roughness.

2.3 Heat transfer performance of Nano-fluid

In recent years, a better heat transfer performance of Nano-fluid as coolant has drawn more and more attention of the scientists. Basically, Nano-fluids are dilute liquid suspensions of nanoparticles with usually at least one critical dimension of smaller than 100 nm. The common particles are Al_2O_3, Cu, ZnO andTiO_2 while common base fluid are oil, water or ethylene glycol. The enhanced thermal behavior of nano-fluids motivates scientists to explorer better solutions on the fields like power plant, micro-manufacturing and ventilation and air-conditioning.

Experiments have shown that when nanoparticles are added into the traditional heat exchanger working fluids, their thermal properties changes especially the effective thermal conductivity of the nano-fluids increases. Different empirical models have been suggested to predict effective thermal conductivity based on experimental data. H.Xie etc (Nanoscale Research Letters) conducted a series of experiment on performance of nanofluid and conclude the following factors which can affect the thermal performance of the nanofluid:

Volume fraction of nanoparticles, the tested temperature, thermal conductivity of the base fluid, nanoparticles size and additives of the fluids.

For the nano-fluid preparation, suspension of the nano-particles is most important. S. Zeinali Heris, M. Nasr Esfahany and S. Gh. Etemad (2006) mixed distilled water and solid nanoparticles Al_2O_3 in concentration of 0.2%, 0.5%, 1.0%, 1.5%, 2.0%, 2.5% after circulation and then vibrated for 8-16 hours in ultrasonic mixer system (model Parsonic 3600 S). None of these nano-fluids had sedimentation after 24 hours which provided average distribution of the nanoparticles in the solvent. Also they set up a flow loop consisting of several measuring sections for temperature, pressure and flow rate to investigate the convective heat transfer performance of the nano-fluid in the laminar flow. Their work showed that with the increase of concentration of the nanoparticles and Reynolds number in nano-fluid, heat transfer coefficient increases. One of the important result is that the increase in thermal conductivity of nano-fluid is not the only reason for heat transfer enhancement in nano-fluids. Other factors such as dispersion, chaotic movement of nanoparticles, Brownian motion and particle migration also have influence on augmentation of the heat transfer of the nano-fluid. In the paper by Sidi El. Becaye Maiga (2004), the author investigated the hydrodynamic and thermal behaviors of nano-fluid flowing inside a uniformly heated tube. Results showed the increasing particle volume concentration are accompanied with drawback on the wall shear stress. Also they found the ethylene glycol - Al_2O_3 gave better heat transfer enhancement than the water- Al_2O_3 nanofluid under same concentration.

Using multi-current hot-wire technique, Jose R. and Vázquez Peñas etc(2008) presented experimental results of the thermal conductivity of several nano-fluids prepared

by dispersing nanoparticles of SiO_2 and CuO in the based fluid of ethylene glycol and water with different concentrations up to 5% in mass fraction. Their experimental technique allowed a pretty accurate determination of the enhancement in the thermal conductivity of the fluids due to the presence of dispersed nanoparticles. Their test results come close in correspondence with some of their theoretical calculation but in some cases the difference between them is very large. Yajie Ren, Huaqing Xie and An Cai (2005) used theoretical model which includes considerations of the effects of an interfacial nanolayer by liquid molecule layering on the particle/liquid interface and of micro-convection caused by thermal motion of nanoparticles to predict enhancement in effective thermal conductivity of a nanofluid with respect to the suspended nanoparticle size, volume fraction, temperature, thermal conductivities of the nanoparticles and base fluid. The test fluid they use are Cu-Ethylene Glycol(EG) , Al_2O_3-water and CuO-EG nanofluid. The calculated values fit quite well with some currently available experimental data.

CHAPTER 3

EXPERIMENTAL FACILITY

3.1 Single Heater Element Loop Tester

Sponsored by Westinghouse, a Single Heater Element Loop Tester (Figure 3.1) was built at Department of Mechanical Engineering at University of South Carolina-Columbia. This loop is for the purpose of investing the proposed design modification of the simulated fuel rod. The thermal hydraulic loop can deliver up to 14.3 m^3/ hr of flow rate for the DI-water and 13.85 m^3/ hr for the Nano-fluids. The plugged rotary pump (0.75 HP Grundfos model CRIE 10-1 unit) is used to pump the working fluid through the whole loop. The pump has a cool-top air-cooled shaft seal chamber that enables it to handle the fluid up to 356°F. The SHELT loop(Figure 3.1), entirely thermally insulated, is a closed and thermally insulated loop with one bypass, shell and tube type heat exchanger and a vertical test section where the simulated fuel rod is located inside. The fuel rod is connected to a 10 kilowatt power supply.

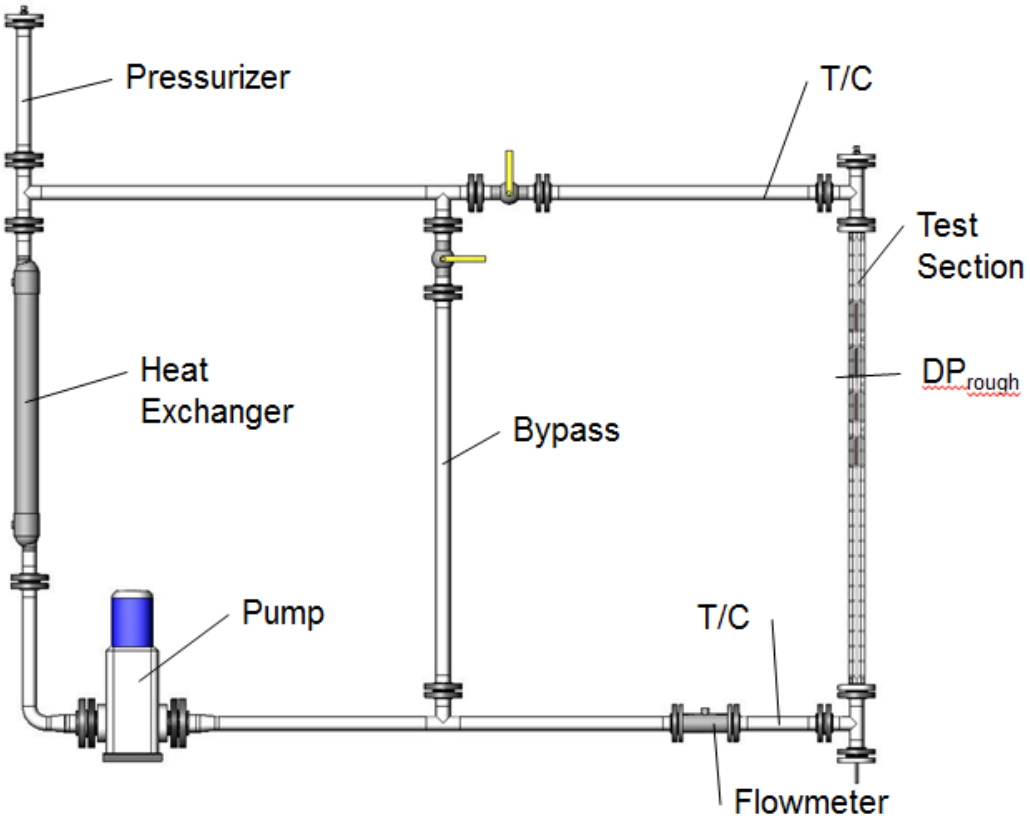

Figure 3.1: The SHELT loop

3.2 Pump

The pump used to circulate the fluid throughout the loop is of 0.75 HP with brand Grundfos model CRIE 10-1 unit. It is a vertical inline multi-stage booster pump that can deliver 14.3m^3/ hr of flow rate against a 10 m head for water and 14.02m^3/ hr for 0.5% nanofluid and 13.85m^3/ hr for 2%nano-fluid. Also the pump is designed to have a cool-top air-cooled shaft seal chamber that allows it to handle up to 185°C of the fluid temperature.

3.3 Pressure Transducers and Air compressor

Three Rosemount 2051Cd differential pressure transducers (4-20 mA/62.3 kPa) are connected to the test section in order to give the differential pressure drop at the smooth and rough surface. These transmitters are calibrated as the following span:

1. 0 ~ 2 kPa

2. 0 ~ 4 kPa

3. 0 ~ 5.33 kPa

Another Rosemount 2051CG pressure transducer is located outside the test section to measure the pressure of the whole loop. It can convert signal up to 2.07Mpa.

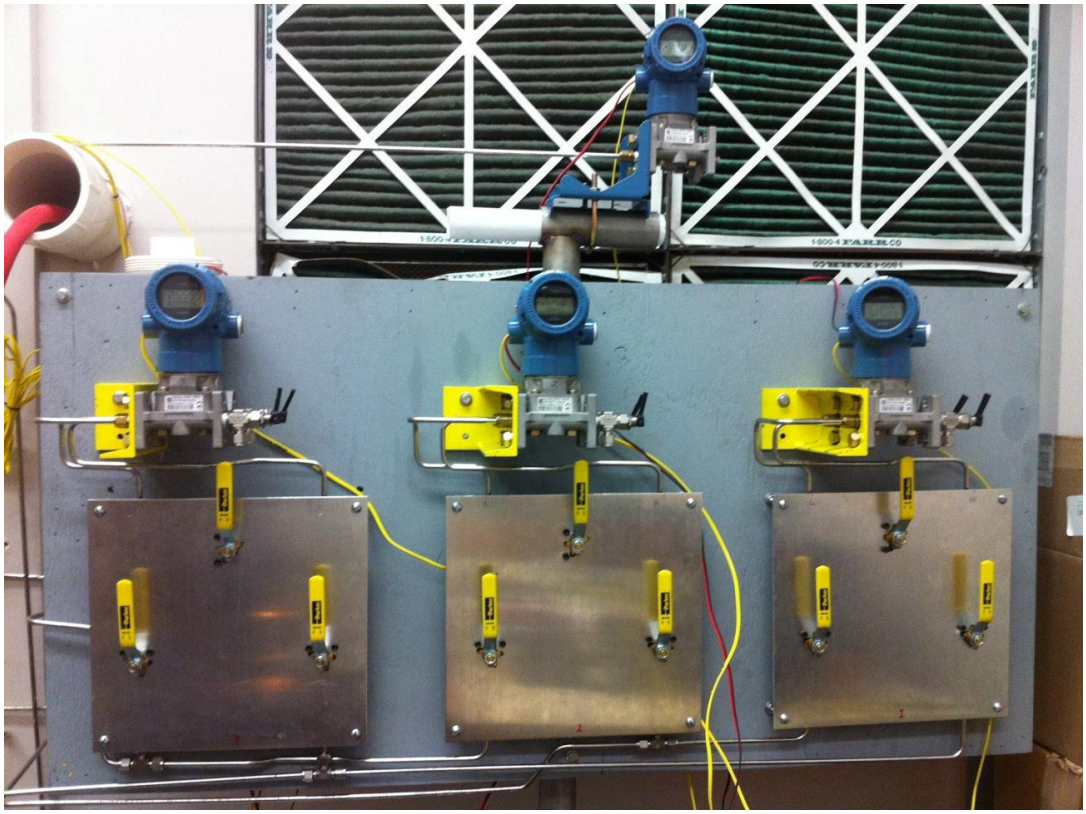

Figure 3.2: Differential Pressure Transducers

All these four pressure transducers are installed with bleeder valves which not only can maintain the desired pressure but also eliminate the air bubbles from the system to minimize experimental error. Also for the same purpose there is a bleeder valve at the top

of the test section. All the pressure transducers are connected to the DAQ(DATA ACQUISITION) system. The reading from all the gauges are recorded into the system.

A 0.026 m3 and 0.9 MPa compressor is being used to pressurize the system for cold test. The pressurizer is constructed from 304 stainless steel piping partially filled with water above the loop. Approximately 0.0508 ~ 0.1016 m empty space is left at the top of the pressure column to pressurize the loop after the heat been put into the rod.

3.4 Thermocouples

Two OMEGA thermocouples (K-types) are inserted in the test section, the tips of the thermocouple are maintained in the middle of the pipe. The two thermocouples are devoted to read the temperature of the coolant both inlet and outlet of the test section.

In order to determine the average temperature of the rough section, two additional sliding thermocouples are located inside the rod, these thermocouples press against the inner walls of the test section on two sides. These two thermocouples are bundled at a sliding probe that are free to move vertically inside the rod, providing two groups of data of the temperature at the inside surface of the heater rod. Also the thermocouple probe can freely rotate circumferentially.

All the thermocouples are connected to the data acquisition system with LABVIEW 8.6 to for recording of the data.

3.5 Power Supply

As figure 3.3 shows, these two III-Phase DC power supplies are used to provide power for providing joule heating the rod. The maximum power it can supply is 10 KW, at 500 Amps and 20 Volts. Joule heating by passing electrical current through the test section is used to heat up the rod and the circulating coolant is heated by the surface heat flux of the rod.

According to the property table the electrical resistance of Inconel tubing is 32.3 kΩ and Nickel Rod and tubing are only 3.8 kΩ. Therefore the resistance heating of the Nickel Rod is negligible compared to the Inconel Tube and account for its heating effects inside the test section.

Figure 3.3: Power supple

In addition to volt meter amp meter, for measuring the voltage and current flow of the power supply, we use a clamp meter (600A Fluke 375) to measure the power on the test section for accuracy of measurement.

Bushings are being covered in the top and bottom flanges that hold the rod. The purpose of this is to electrically insulate the test-section from the rest of the test loop. To reduce the energy loss from the outer surface of the test loop, thermal insulation is used to cover the outer surface of the whole loop.

3.6 Heat Exchanger

In order to maintain the desired temperature in the loop, a shell and tube type heat exchanger (Single-phase, 76 mm diameter) is being used. Fresh water from the tap is flowed into the heat exchanger to cool down the loop. To regulate the flow a 19mm sophisticated precision valve is used, which is made of brass. The regulating valve is installed at the outlet of the heat exchanger with a flow meter installed on the hose water line to take readings of the fresh water flowing into the heat exchanger. By regulating the cooling water flowing into the heat exchanger we can get the desired inlet temperature of the whole test loop. A flow meter (Rate Totalizer F-1000-RT) is installed at the inlet of the Heat exchanger to measure the flow rate. The flow meter can measure accurately over a range of 0.1816 m3/ hr ~ 1.8169 m3 / hr.

3.7 Coolant

The coolant used in the loop is DI (deionized) -water, 0.5% ZnO-DI-water based nano-fluid and 2% ZnO-DI-water based nano-fluid. DI-water is obtained from the laboratory in

Chemical Engineering Department of University of South Carolina- Columbia. We use DI-water to avoid impurity inside the loop which can affect the test results.

The 2% Nano-fluid are purchased by Mechanical Engineering Department. The 0.5% Nano-fluid mixture is prepared from 2% Nano-fluid by adding DI-water in proper volume percentage after calculation. Before the nano-fluid was introduced into the loop the mixture is well shaken to ensure the homogeneity of the solvent. During the experiment the fluid is circulating through the loop, which keeps the nano particles in homogeneous suspension.

3.8 Test Rod

The total length of the test rod is 2.1526 m. It is made of two kinds of metals. The bottom half and upper part of the rod is Nickel. In the middle there is a 0.5334 m long Inconel tube. All the three parts are brazed together in the workshop using white flux brazing paste and SA45 Brazing wire. The bottom part of the fuel rod is a solid nickel rod while middle and upper part of the rod are tubes. The outer surface diameter of the tube is 9.5mm, the inner diameters of tubes is 8mm. So the wall thickness is 1.5mm. The rough region on the Inconel part of the rod has 0.3048 m length on its outer surface. The three dimensional roughness is a diamond shape that is formed on to the Inconel tube at Machine shop using a Coarse knurling tool and a modified Lathe machine. Figure 3.4 shows the heater/fuel rod.

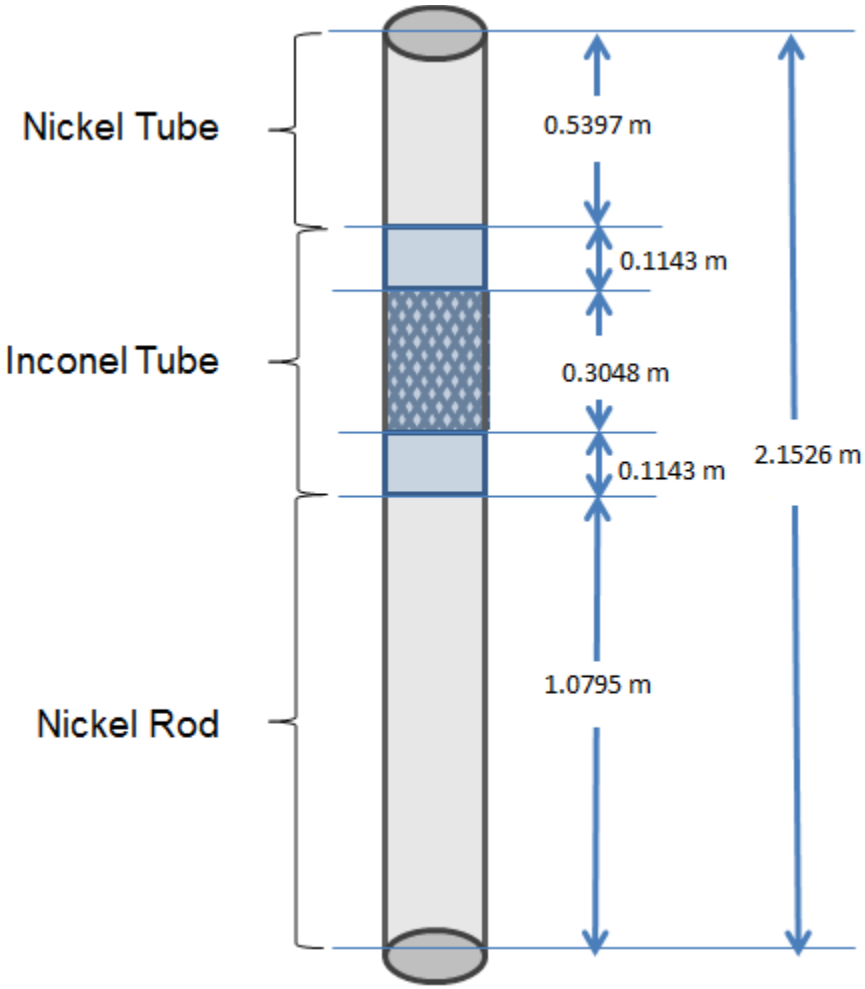

Figure 3.4: Properties of the test rod

To keep the alignment of the rod inside the test-section, we use Eight Ultra-high temperature Ceramic rods with a diameter of 3.175mm and a length of 5cm. Two groups of four ceramic rods are respectively held in fittings that are machined and welded into on the test section. All the eight ceramic rods are used to fix the rod into the center of the test-section. The alignment of the test rod is being confirmed when the circumferential temperature readings from the heater rod during the thermal test does not vary more than 0.5 degrees from point to point. To eliminate the entrance effects on the result the trailing

edge of the Inconel rod was located at a distance of more than 25 Hydraulic Diameters from the coolant inlet to the test-section. The leading edge of the Inconel rod is more than 15 Hydraulic Diameters from the top end at the tee-joint.

The annular test section which contains the simulated rod is totally 1.524 m long with an inner diameter of 38.1c m. It has been welded with flanges at both sides in Machine Shop in order to fit the loop. Its flow housing is made from ASTM B241 aluminum tube. The test section has a wall thickness of 6.35mm. The cross section is as shown in Figure 3.5.

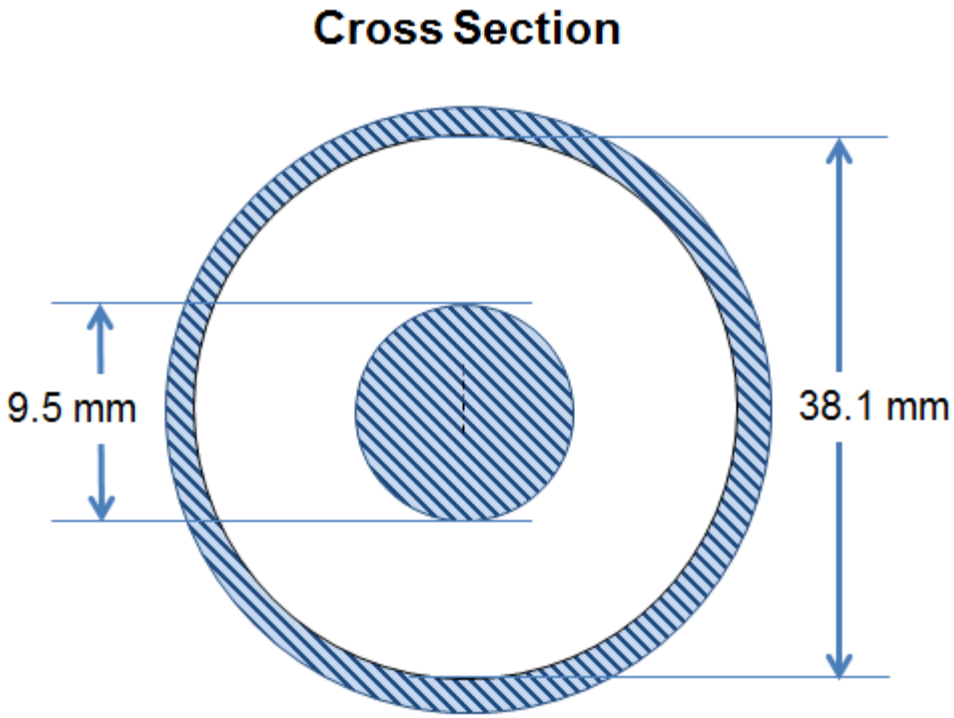

Figure 3.5: Cross Sectional view of Test Section

3.9 Flow Regulation

The flow in the test section is regulated by two valves, as the figure shows, one on start of the test section and the other on end of the test section. While the flow from pump is

constant, we use the valves to by-pass the flow and get the desired flow rate through the test section. The total volume of test loop is 0.021 m^3. For the current study 3 different flow rates for each group of thermal tests were used, these being 4.08 m^3 / hr, 9.06 m^3 / hr and Maximum flow rate pump can provide. A Flowmeter (MCII- Flow Analyzer NUFLO) is installed before the test-section to measure the flow going into the Test-section.

3.10 Processing system

The hardware for the processing system is National Instruments (NI DAQ-9172) Data Acquisition System as shown in Figure 3.6, which is connected to a computer. NI-9172 DAQ card is used to convert voltage signals from thermocouples and NI-9203 DAQ card is used to convert signals from pressure transducers into readings that are collected and stored by the computer.

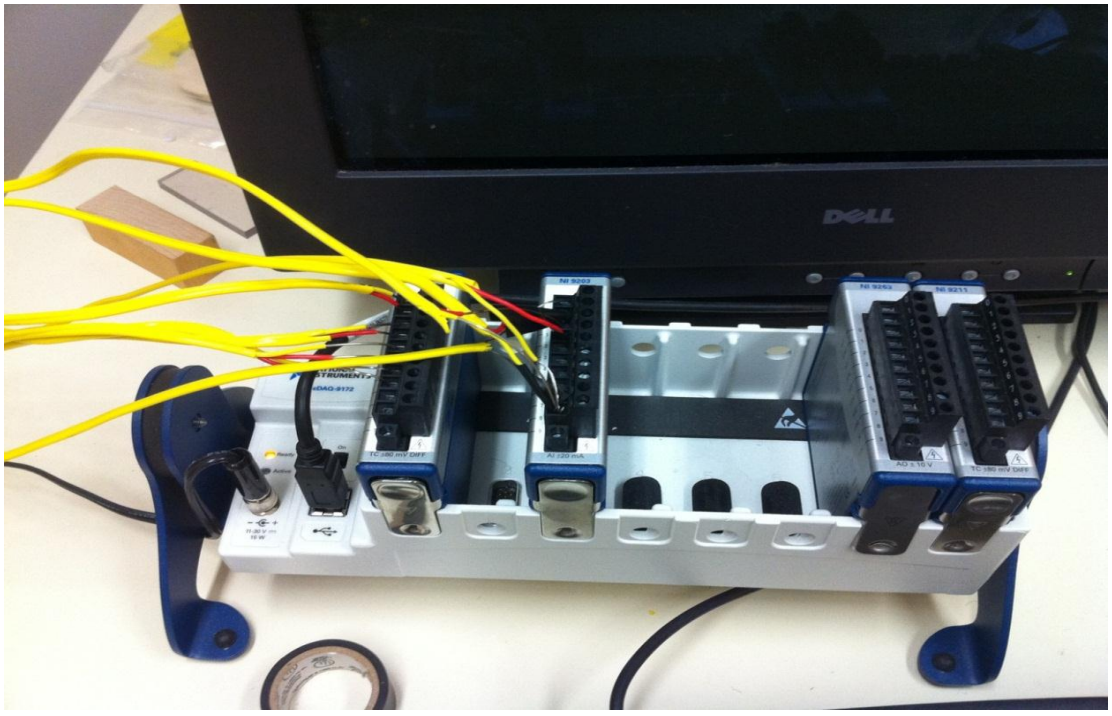

Figure 3.6: Data Acquisition System

The software used to collect the data is Lab View 8.6 based on 32-bit Window XP. Figure 3.7 is the screenshot of the Lab View 8.6 display.

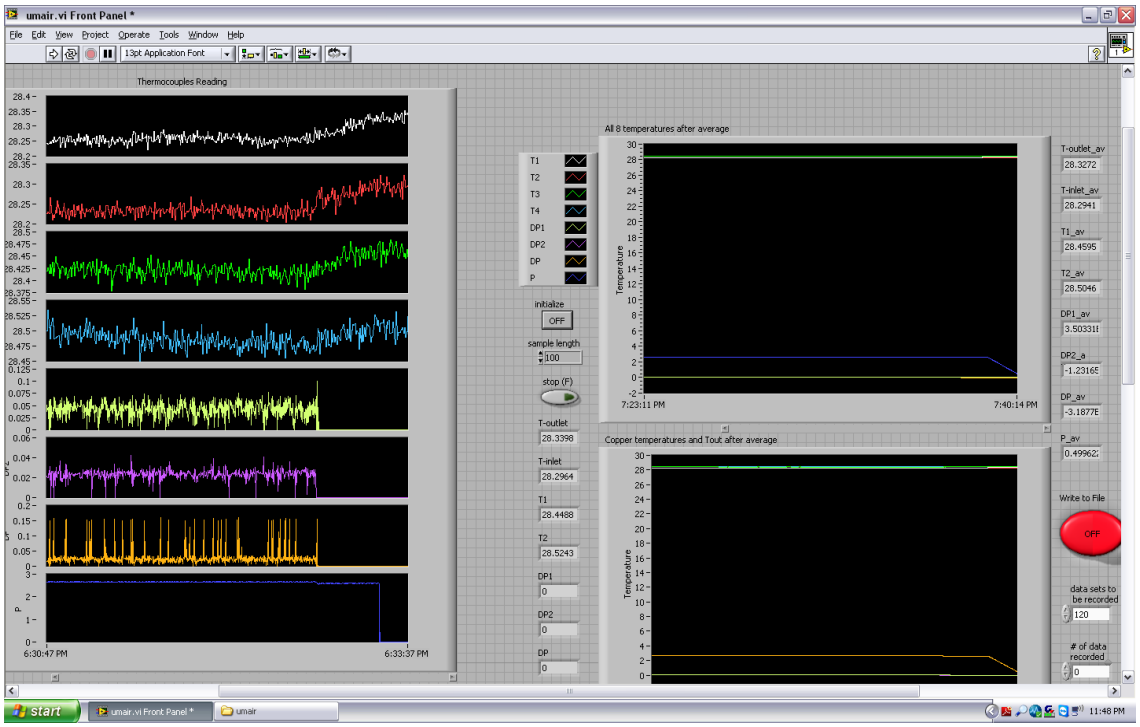

Figure 3.7: A screenshot of Labview 8.6

3.11 Geometry of the Roughness

For 3-Dimensional roughness (Figure 3.8), the total rough section on the Inconel part is 0.3048m in the middle which left the smooth section of Inconel part 0.1143m on either side. As Figure 3.8 shows, the roughness has a continuous diamond shape pattern. The angle of the corrugation at each diamond is 45 degrees with a length of side 1mm. The depth of the roughness is 0.3mm and pitch of pattern is 1.614mm. Between each two diamond is 0.2mm.

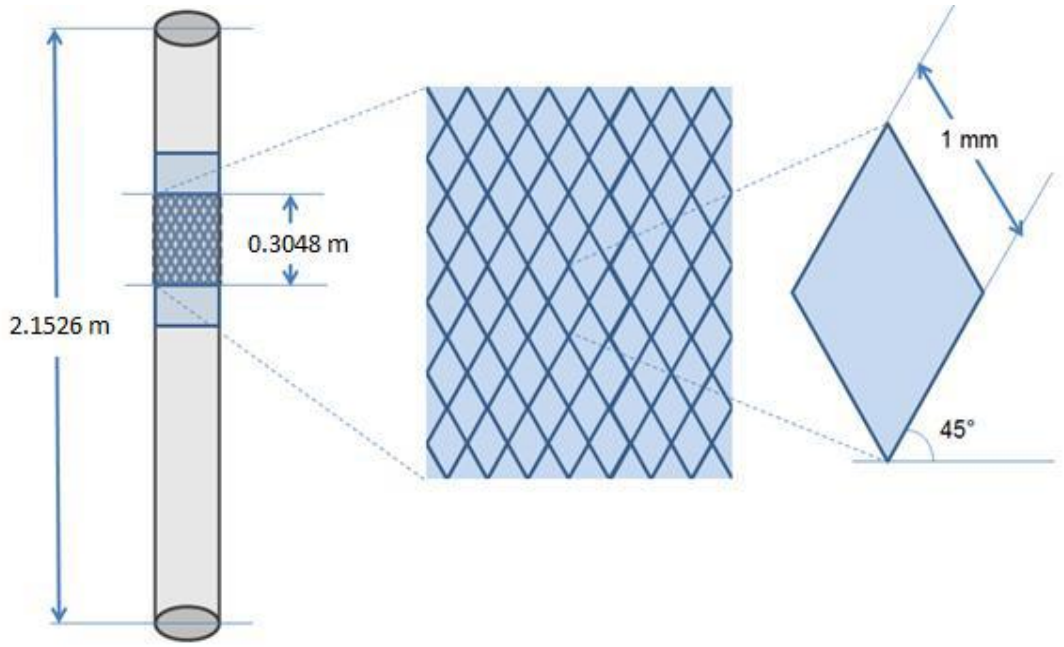

Figure 3.8: 3-D Surface Roughness Geometry

CHAPTER 4

TEST PLAN

4.1 Steady State Condition

The data recorded for the tests are all after the experimental parameters have reached complete steady state. Normally the steady state are reached hours after each test starts and only after that the data is recorded. We assume that when the temperature difference of the Inconel rod between the beginning and the end of the record is less than 0.5 ^{o}C, we have reached steady state. Before any test, valve is opened to let coolant (tap water) flow into the heat exchanger. This valve can read flow rate precisely and keeps the flow constantly as well. Desired loop temperature is obtained by adjusting the power supply into the rod. After heat is put into the rod and the flow rate of the heat exchanger has been fixed, it usually takes 2-4 hours to reach the steady state. When the pressure and the temperature are stable, we start to collect the data.

4.2 Cold Test

Cold test is a must before each thermal test to get the pressure drop and frictional losses in the test section. This procedure is to make sure that there is no leakage in the loop and everything is ready for the thermal test. At this procedure, no heat input is needed.

4.3 Thermal Test

For 3-dimensional roughness, after the flow reached steady state, we begin recording the data from the first data point which is 0.0254 m from the start of rough section at the inner

surface of the rod. This first data point is defined as smooth section point. Then the total rough section is divided into six set of data points at equal distance apart. For every axial point, there are two temperature reading from the thermocouple.

The recorded data for each test also include the flow rate of the coolant, flow rate of heat exchanger, pressure drop and overall pressure of the loop for each group of test. For each of coolant and a fixed temperature, three different flow rates through the test section is being used to study the effect of flow rates on heat transfer, these flow rates being 4.54 m3/ hr, 9.08 m3/ hr and maximum flow rate the pump can provide. Also for each data point at rod, we record a total of 180 readings through LABVIEW which record 6 readings every second for 30 seconds. A total of 8 thermal tests will be run at a rage of:

- Bulk Temperature: 60 and 70 °C
- Rod temperature: 85 ~ 165 °C
- System Pressure: 0.45 ~ 0.55 MPa
- Power: 0 ~ 10 KW
- Water flow rate: 4.54 ~ 14.3 m3 / hr
- Differential pressure: 0.029 ~ 0.29 psi

4.4 Test Parameter Tolerances

- Rosemount pressure Transducers: +/- 0.075% of span. (Range: 0.2 kPa ~ 2 mPa)
- Cameron NUFLO flow-meter: +/- 0.5% of reading. (Range: 3.4 ~ 80 m3 / hr)
- Thermocouples: +/- 0.2 °C of reading. (Range: 0~1250 °C)
- Power Supply: +/- 0.22 KW (Range: 0~10 KW)

4.5 Uncertainty Analysis

The uncertainty analysis was conducted according to procedure in Coleman and Steele (2009). Measurement uncertainties and tolerance for thermocouples, flow rate meter, clamp meters were taken into calculation. The following equation is adopted to get the uncertainty of the heat transfer coefficient:

$$b_h^2 = \left(\frac{\partial h}{\partial V}\right)^2 b_V^2 + \left(\frac{\partial h}{\partial I}\right)^2 b_I^2 + \left(\frac{\partial h}{\partial T_s}\right)^2 b_{T_s}^2 + \left(\frac{\partial h}{\partial T_b}\right)^2 b_{T_b}^2$$

Where b_h is the uncertainty in heat transfer co-efficient and b_V , b_I , b_{T_s}, b_{T_b} are the uncertainties associated in the measurement of voltage, current and temperature of surface of the rod and bulk temperature.

The average uncertainty for heat transfer coefficient associated with water is +/- 1.25 % with a maximum uncertainty of +/- 3.145 % for thermal test at 70 ℃ with 3-dimensional roughness at **Re**=2.67e5. The average uncertainty for heat transfer coefficient associated with 0.5% nano-fluid using 3-dimensional roughness is +/- 1.79 % with a maximum uncertainty of +/- 5.318 % for thermal test at 70 ℃ at **Re**=1.35e5. The average uncertainty for heat transfer coefficient associated with 0.5% nano-fluid using 2-dimensional roughness is +/- 1.92 % with a maximum uncertainty of +/- 4.538 % for thermal test at 70 ℃ at **Re**=2.10e5. The average uncertainty for heat transfer coefficient associated with 2% nano-fluid with 3-dimensional roughness is +/- 1.25 % with a maximum uncertainty of +/- 2.993 % for thermal test at 80 ℃ at **Re**=1.15e5.

CHAPTER 5

DATA REDUCTION

The rate of Convective heat transfer through the test-section was determined by heat balance equation:

$$Q = \dot{m} * C_p(T_0 - T_i) \qquad (5.1)$$

$\dot{m}$ is the mass flowrate across the test-section, C_p is the heat capacity of the coolant at set pressure, T_0 and T_i are the temperature of the fluid at the outlet and inlet of the test-section. Here the properties of fluid were all employed at average temperature of the fluid:

$$T_m = \frac{(T_0 + T_i)}{2} \qquad (5.2)$$

Where T_i and T_0 are fluid temperatures at inlet and outlet of the test section. The amount of total heat input to the test section from power supply is:

$$Q_{in} = P = V * I = Q_{in} \qquad (5.3)$$

V and *I* are the voltage and electric current readings read precisely from a Clamp meter at the top and bottom metallic connections of the heater rod. Q_{in} is the total input of power to the test rod. The bulk temperature for this analysis was determined by:

$$T_b = T_i + \frac{Q}{\dot{m} * C_p} * \frac{x}{l} \qquad (5.4)$$

T_i is the inlet temperature of the fluid into the test-section, Q is the rate of convective heat transfer in the test-section , C_p is heat capacity at constant pressure, $\dot{m}$ is the mass flow rate in the test-section. *x* is the elevation of the thermo couple probe which also equals to

the distance of the data point from the beginning of the Inconel rod and *l* is the total length of the Inconel rod of 0.5334m.

The rate of heat generation for the Inconel part of heater tube was calculated considering the electrical resistivity of Inconel into account. To calculate the rate of heat generation for the both parts of the tube, the rate of heat generation equation is applied:

$$Q''' = \rho_e \left[\frac{4I}{\pi(d_0^2 - d_i^2)}\right]^2 \qquad (5.5)$$

Here ρ_e is the electrical resistivity of the material, d_0 and d_i are the outer and inner diameters of the Heater rod respectively and *I* is the current input. To calculate the rate of convective heat transfer for Nickel part, at first the rate of heat generation for the total power of Nickel rod (bottom part of rod) and Nickel tube (upper part of rod) are calculated and then multiplied it with the volume of the Nickel Rod and Nickel tube respectively and then get the convective heat transfer for Nickel part of the rod to calculate the heat losses.

For these experiments the thermal couples read the temperature of the inner surface of the rod for at rough section, so the following conduction formula is used to calculate the temperature at outer surface of the rod:

$$T_{w,0} = T_{w,i} + \frac{Q'''}{16k}\left(2d_i^2 \ln\frac{d_i}{d_o} - d_i^2 + d_o^2\right) \qquad (5.6)$$

Where Q''' is the rate of heat generation in the Inconel tube, *k* is the thermal conductivity of the Inconel, d_o & d_i are outlet and inner diameter of the Inconel tube, $T_{w,o}$ and $T_{w,i}$ are the temperature at outer and inner surfaces of the rod respectively.

The total losses of heat from the system were calculated by:

$$Q_{loss} = Q_{in} - Q_{inconel} - Q_{nickel} \qquad (5.7)$$

The hydraulic diameter D_h was calculated by subtracting the inner diameter of the test-section D_i and outer diameter of the heater rod d_o:

$$D_h = D_i - d_o \qquad (5.8)$$

Reynold's Number was calculated using the following equation:

$$Re_{D_h} = \frac{\rho v D_h}{\mu} \qquad (5.9)$$

ρ is the density of the fluid at its mean temperature and μ is viscosity of the fluid at same temperature, v is the velocity of the fluid in the test section. Velocity in the test section was determined using:

$$v = \frac{\cancel{Q}}{A_h} \qquad (5.10)$$

$\cancel{Q}$ is the flowrate of the fluid and A_h is the area of cross section in the test-section. Mass flow rate $\dot{m}$ in the test-section for each test analysis was determined by following formula:

$$\dot{m} = \rho * v * A_h \qquad (5.11)$$

Where ρ is the density of the fluid, v the velocity of the fluid and A_h is the area of cross section. Heat flux was calculated through the following formula:

$$Q'' = \frac{Q_{in}}{A_s} \qquad (5.12)$$

Where Q_{in} is the total heat input to the Inconel section and A_s is the surface area of Inconel part.

Heat transfer co-efficient, assuming no heat loss, was calculated using the energy balance:

$$h = \frac{Q''}{(T_s - T_b)} \qquad (5.13)$$

Where Q'' is the total heat flux, T_s is the temperature of outer-surface of the rod and T_b is the bulk temperature of fluid at different elevation of the rod. Lastly Nusselt number was calculated using the following formula:

$$Nu = \frac{hD_h}{k_f} \qquad (5.14)$$

Where h is the heat transfer co-efficient, D_h is the hydraulic diameter and k_f is the thermal conductivity of the coolant at the mean fluid temperature. For thermal conductivity of nanofluid, we use the empirical equation of Jose R. Vazquez Penas(2008):

$$\frac{1}{\lambda_{eff}} = \frac{\phi}{\lambda_p} + \frac{1-\phi}{\lambda_f} \qquad (5.15)$$

Where λ_{eff} is the effective thermal conductivity of nanofluid. λ_p is the thermal conductivity of nanoparticles and λ_f is the thermal conductivity of the pure base fluid. ϕ is the volume concentration of the nanoparticles.

Heat transfer coefficients were calculated for all three kinds of coolant using same formula and were then compared for each case. The HT_{enh} heat transfer enhancement of different comparison group in the rough region was calculated as follows:

$$HT_{enh} = \left(\frac{h_1}{h_2} - 1\right) * 100 \qquad (5.16)$$

Where $h_1$and h_2 are the heat transfer co-efficient of the two different kinds of coolant.

CHAPTER 6

EXPERIMENTAL RESULTS & DISCUSSION

6.1 Comparison of heat transfer co-efficient for different fluids

Thermal tests were conducted for comparison of heat transfer enhancement using nano-fluids as coolant versus DI-water as a coolant. For each test a pre-determined temperature of the working fluid and fuel rod was achieved at a flow rate of 4.54 m^3/ hr. Before recording any data, the test was run until a steady state condition was achieved. After recording the first set of data, the flow rate was increased to 9.08 m^3/ hr. Steady state was again achieved before recording the next set of data .The same procedure was followed for third group of data recoded at 14.3 m^3/ hr, which is the maximum flow rate provided by the pump. During each the thermal test, all the parameters are kept the same while the flow rate is the only parameter changed. Two different water inlet temperatures with 3-D roughness at 0.5 % and 2% nanoparticle concentrations were investigated. Additionally 2-D roughness was also evaluated at 0.5% nanoparticle concentration. The results from the experimental study are presented below.

Comparison Group# 1

The test conditions for first group of thermal test are:

- Fluid Inlet Temperature: 70 °C
- Power: 2.88 KW

- System pressure: 0.33 ~ 0.55 MPa
- Flow rate: 4.5 m^3/ hr, 9.08 m^3/ hr, max fluid rate respectively
- Roughness: 3-Dimensional

The surface temperature drop across the rough region of the fuel rod for all fluids used in experiments was recorded. Taking all the parameters into account the calculations for heat transfer co-efficient were conducted.

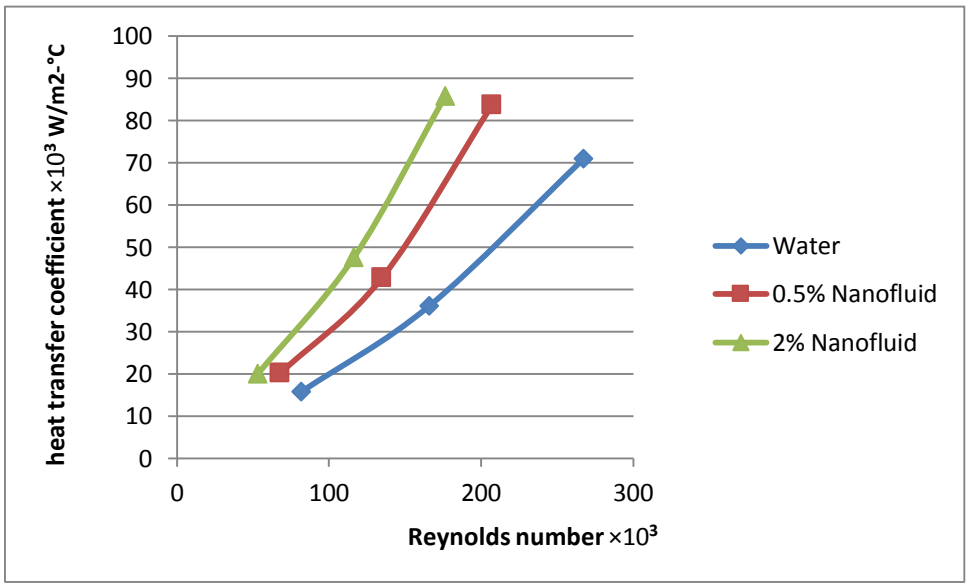

Figure 6.1: Heat transfer coefficient **h** at different Reynolds number @70°C

Figure 6.1 presents a comparison of heat transfer co-efficient calculated for three different fluids. It is evident from the graph that 2% ZnO nano-fluid gives the highest heat transfer co-efficient values compared with 0.5% ZnO nano-fluid and DI-water. These results were expected due to higher effective thermal conductivity at 2% concentration, and are supported by literature review done by the author.

Comparison Group#2

The test conditions for second group of thermal test are:

- Fluid Inlet Temperature: 80 °C

- Power: 3.98 KW
- System pressure: 0.33 ~ 0.55 MPa
- Fluid rate: 4.5 m^3/ hr, 9.08 m^3/ hr, max fluid rate respectively
- Roughness: 3-Dimensional

For this thermal test we had 8°C to 9°C of temperature drop across rough section. The Bulk temperature was raised by 0.5°C across the test section.

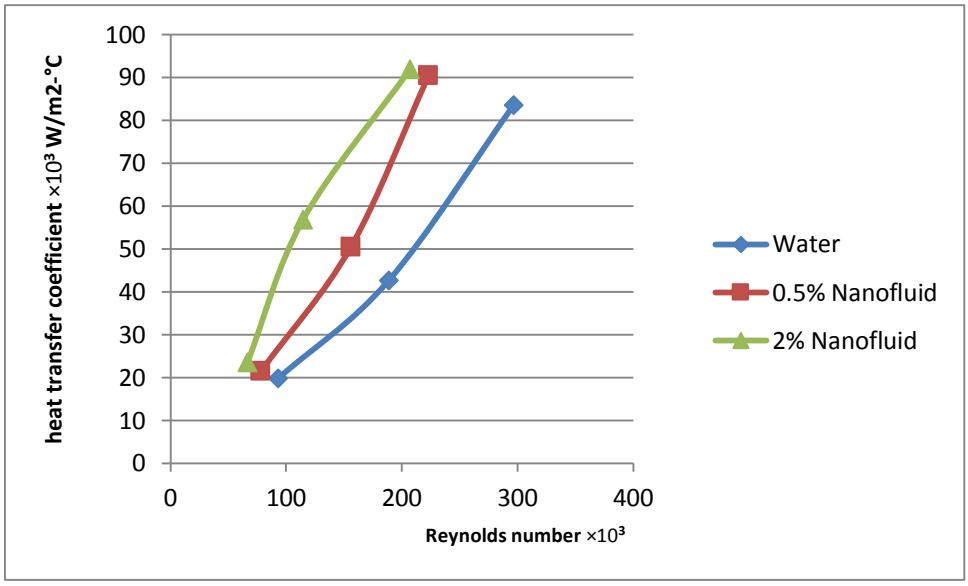

Figure 6.2: Heat transfer coefficient **h** at different Reynolds number @80°C

Figure 6.2 illustrates the heat transfer co-efficient for different fluids with various Reynolds' number at rough section. Since the bulk temperature for this thermal test was higher than the previous test so the resulting heat transfer enhancement in rough surface region was also recorded higher compared to previous test at all **Re**.

6.2 Comparison of heat transfer co-efficient with different roughness

Comparison Group#3

The test conditions for third group of thermal test are:

- Fluid Inlet Temperature: 70 °C

- Power: 2.88 KW
- System pressure: 0.33 ~ 0.55 MPa
- Fluid rate: 4.5 m^3/ hr, 9.08 m^3/ hr, max fluid rate respectively
- Roughness: 3-Dimensional & 2-Dimensional
- Fluid type : 0.5% water-based ZnO nanofluid

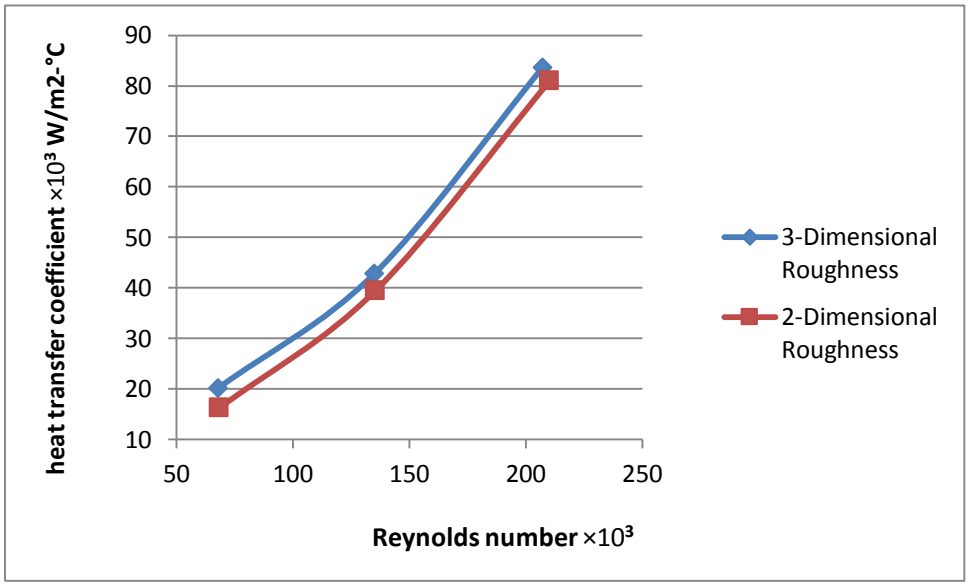

Figure 6.3: Heat transfer coefficient **h** for different Roughness geometry @70°C

Figure 6.3 presents a comparison between the heat transfer co-ffecient as a function of Reynolds's number for two different types of surface geometries i-e, 2-dimensional surface roughness and 3-dimensional surface roughness. It is evident from the figure that 3-dimensional surface roughness gives better heat transfer than 2-dimensional surface roughness.

Comparison Group#4

The test conditions for third group of thermal test are:

- Fluid Inlet Temperature: 80 °C
- Power: 2.88 KW

- System pressure: 0.33 ~ 0.55 MPa
- Fluid rate: 4.5 m^3/ hr, 9.08 m^3/ hr, max fluid rate respectively
- Roughness: 3-Dimensional & 2-Dimensional
- Fluid type : 0.5% water-based ZnO nanofluid

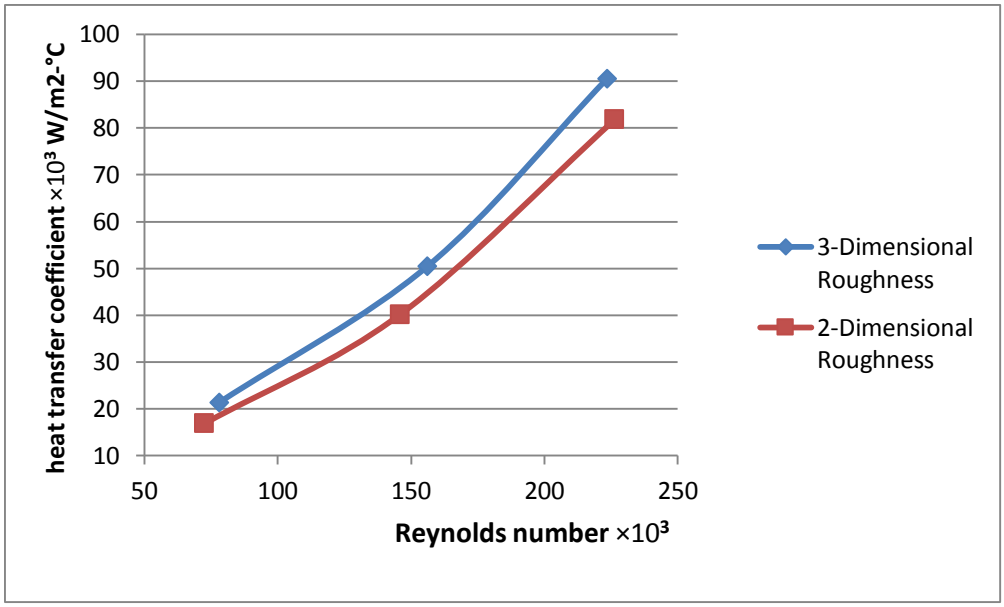

Figure 6.4: Heat transfer coefficient **h** for different Roughness geometry @80°C

Figure 6.4 presents a comparison between the heat transfer co-ffecient as a function of Reynolds's number for two different types of surface geometries i-e, 2-dimensional surface roughness and 3-dimensional surface roughness. Similar trend of higher heat transfer co-efficient for 3-dimensional surface roughness was observed in this thermal test.

6.3 Variation of Nusselt number as a function of Reynolds number

In this section a comparison is being presented for the variation of Nusselt number as a function of Reynold's number. 3-dimensional surface roughness geometry was used for these thermal tests. These tests were conducted at two different temperatures.

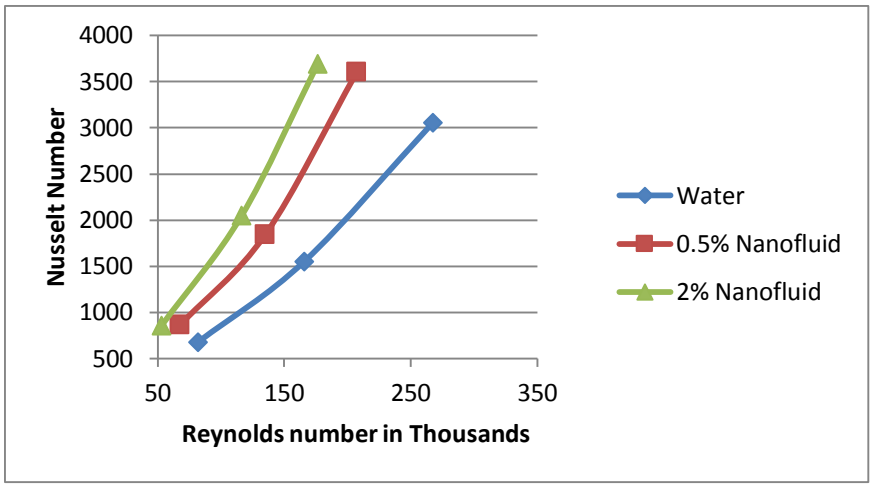

Figure 6.5: Nusselt number (**Nu**) at different **Re** @70 °C

Figure 6.5 shows a variation of average Nusselt number (Nu) as a function of Re for the first thermal test across the test-section. From the experimental results it is evident that Nu increases as we go at higher Re in fuel rod bundles. The heat transfer co-efficient increases significantly as we increase the flow-rates i-e at higher Re. It was observed during the experiments that as the Re increases the bulk temperature also increases and the rod temperature decreases, resulting in higher heat transfer co-efficient.

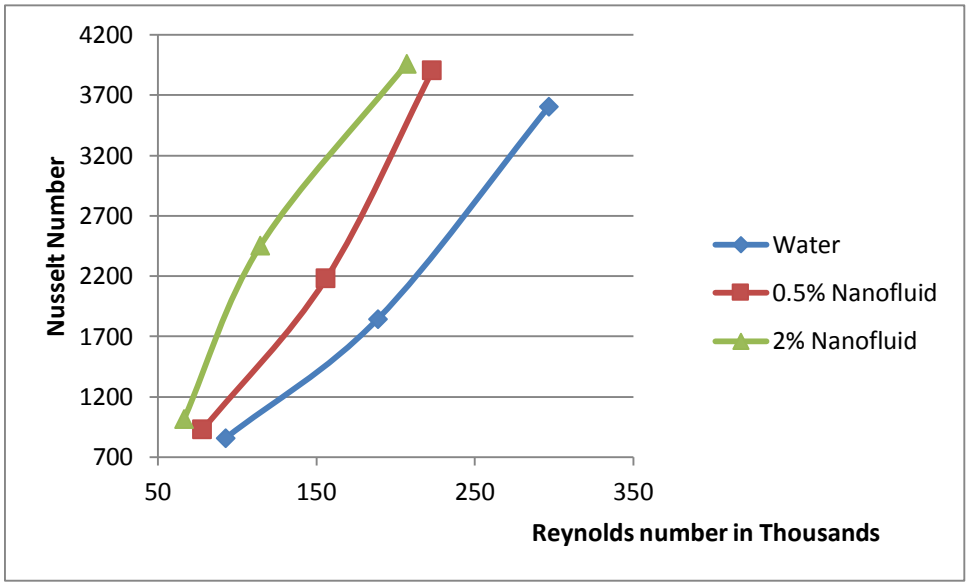

Figure 6.6: Nusselt number (**Nu**) at different **Re** @80°C

Figure 6.6 shows a similar variation of **Nu** as the **Re** increases. The **Nu** is not a constant value as the flow is still thermally developing regime especially at higher **Re**. Since the convective heat transfer co-efficient is proportional to the coolant flow across the fuel rod, so higher **Re** results in higher **h** values thus higher **Nu**. For the two Nu-Re graphs, the curve should not be continuous as the flow is turbulent. These curves are just showing the trend of Nu as Re increases.

6.4 Tables

The experimental results are also presented in tabular form in this section.

Table 6.1:Thermal Test Data Analysis of 2% Nano-fluid @70°C with 3-D roughness

Re	Coolant T bulk °C	Rod Ts,o °C	ΔT °C	Q''' (W/m^3)	h (W/m^2 °c) (nanofluid)	h (W/m^2 °c) (water)	Δh Enhancement % compared to DI-water
53200	70.41	80.07	9.65	2.80E+08	2.00E+04	1.58E+04	26.42
116000	71.93	75.99	4.06	2.80E+08	4.75E+04	2.38E+04	31.74
177000	74.26	76.01	1.74	2.80E+08	8.58E+04	7.09E+04	20.95

Table 6.2: Thermal Test Data Analysis of 2% Nano-fluid @80°C with 3-D roughness

Re	Coolant T bulk ℃	Rod \ Ts, o ℃	ΔT ℃	Q''' (W/m^3)	h (W/m^2 ℃) (nanofluid)	h (W/m^2 ℃) (water)	Δh Enhancement % Compared to DI-water
6.65E+04	80.81	91.96	11.16	3.8E+08	2.36E+04	1.98E+04	18.95
1.15E+05	81.87	85.31	3.45	3.8E+08	5.69E+04	4.27E+04	33.2
2.07E+05	82.39	84.98	2.6	3.8E+08	9.19E+04	8.36E+04	9.97

Table 6.3: Thermal Test Data Analysis of 0.5% Nano-fluid @70°C with 3-D roughness

Re	Coolant T bulk °C	Rod Ts,o °C	ΔT °C	Q‴ (W/m^3)	h (W/m^2 °c) (nanofluid)	h (W/m^2 °c) (water)	Δh Enhancement % compared to DI-water
6.78E+04	70.76	80.74	9.99	2.91E+08	2.02E+04	1.58E+04	27.49
1.35E+05	72.44	76.83	4.39	2.91E+08	4.28E+04	2.38E+04	18.58
2.07E+05	73.11	75.27	2.16	2.91E+08	8.36E+04	7.09E+04	17.97

Table 6.4: Thermal Test Data Analysis of 0.5% Nano-fluid @80°C with 3-D roughness

Re	Coolant T bulk ℃	Rod \ Ts, o ℃	△T ℃	Q''' (W/m^3)	h (W/m^2 ℃) (nanofluid)	h (W/m^2 ℃) (water)	△h Enhancement % Compared to DI-water
70200	80.26	98.91	18.65	3.8E+08	2.15E+04	1.98E+04	8.15
146000	82.13	92.71	10.58	3.8E+08	5.05E+04	4.27E+04	18.78
218000	84.12	91.73	7.59	3.8E+08	9.05E+04	8.36E+04	8.31

Table 6.5: Thermal Test Data Analysis of 0.5% Nano-fluid @70°C 2-D roughness and comparison with 3-D roughness

Re	Coolant ° C T bulk	Rod Ts,o °C	ΔT °C	Q‴ (W/m^3)	h (W/m^2 °C) 2-D roughness	h (W/m2 °C) 3-D roughness	Δh Enhancement % comparison 3-D vs 2-D roughness
6.84E+04	70.19	85.37	15.18	2.80E+08	1.62E+04	2.02E+04	24.23
1.35E+05	71.43	80.08	8.65	2.80E+08	3.95E+04	4.28E+04	8.47
2.10E+05	72.74	78.72	5.98	2.80E+08	8.10E+04	8.36E+04	3.28

Table 6.6: Thermal Test Data Analysis of 0.5% Nano-fluid @80°C 2-D roughness and comparison with 3-D roughness

Re	Coolant ° C T bulk	Rod Ts,o °C	ΔT °C	Q‴ (W/m^3)	(W/m^2 °C) 2-D roughness	h (W/m2 °C) 3-D roughness	Δh Enhancement % comparison 3-D vs 2-D roughness
7.27E+04	82.06	101.26	19.21	3.80E+08	1.69E+04	2.15E+04	27.32
1.46E+05	82.13	94.77	12.64	3.80E+08	4.01E+04	5.05E+04	25.88
2.26E+05	83.85	91.36	7.51	3.80E+08	8.18E+04	9.05E+04	10.69

6.5 Nano-Particle Deposition on the rod

It was observed during the experimental investigations that as the fluid inlet temperatures were increased there was deposition of nanoparticles on the rod. Initially at lower temperatures there was no deposition, but as the temperature was increased above 90°C, we suspected deposition of the solids on the surface. This was evident from the insulating effects and rise of rod temperatures, therefore results at temperatures higher than 80°C are not presented, because they are not reliable. A significant amount of nano-particle deposition on the outer surface of the rod was confirmed when the rods were taken out from the test section. The nano-particle deposition was observed on both smooth and rough surfaces of the rod. Nano-particle deposition occurred for 2-dimensional and 3-dimensional surface roughness rods. The maximum deposition occurred on the top end of the rod near the T-section and it decreased as we go towards the bottom end of the rod.

Figure 6.7: Maximum nano-particle depositions

Figure 6.7 shows a maximum deposition that was observed during thermal tests. The layer thickness measured was 1.55mm. This deposition was observed when 2% ZnO nano-fluid was used to conduct the tests for 3-dimensional surface roughness rod.

Figure 6.8: Nano-particle depositions on smooth section of 3-D roughness

Figure 6.8 shows a nano-particle deposition on the smooth section of the rod. Similar trends of deposition layers were observed for both fuel rods. As expected nano-particle deposition layer thickness for 0.5% nano-fluid was lower than for 2% nano-fluid. The maximum layer thickness measured for 0.5% nano-fluid was 0.7mm for thermal tests on 2-dimensional surface rod (Figure 6.9).

Figure 6.9: Nano-particle depositions on rough and smooth section of 0.5% Nanofluid

CHAPTER 7

CONCLUSIONS AND FUTURE WORK

7.1 Conclusions

The objective of this research was to experimentally investigate the enhancement in heat transfer in a simulated nuclear fuel rod bundle using different concentrations of nano-fluids. The results obtained in this study were compared with the experimental results obtained by using different kinds of coolant in a simulated nuclear fuel rod bundle. A SHELT (Single Heater Element Loop tester) setup was used for experimental study. Two simulated fuel rods were used, whose outer surfaces were modified to form three-dimensional and two-dimensional rough surface. A series of systematic thermal tests were conducted. Water based Zinc oxide (ZnO) nano-fluid was employed as coolant for these tests. 0.5% and 2% (Volumetric concentration) ZnO nano-fluids were used to carry out thermal tests. The heat transfer rate with all three kinds of fluids (DI-water, 0.5% nano-fluid, 2% nano-fluid) for rough regions of the rods and then compared with each other. The analyzed data shows the following results:

1. For the same fluid rate, the 2% nano-fluid provides the highest heat transfer co-efficient whereas the DI-water has the lowest heat transfer rate.

2. Heat transfer co-efficient increases as **Re** increases.

3. The maximum heat transfer co-efficient enhancement achieved compared to DI-water was **33%** at **Re=1.15e5** for fuel rod with three-dimensional surface roughness

4. using 2% (volumetric concentration) ZnO nano-fluid.There is severe deposition taken place on top of the test rod which prevent the thermal couple from reading correctly. So test temperature is limited to 80 degrees.

5. The nano-fluid used in this experiment had organic surfactants to facilitate homogeneous mixing of the particles. It is assumed that the surfactants may have broken down at higher temperatures resulting in particle deposition on the solid surface. The second probable cause of particle deposition may also be due to the initiation at collapse of bubles on the rod surface rendering the particles to stick to the surface. A third probable cause of particle deposition may be due to the magnetic field created by the current flowing through the rod.

7.2 Recommendations for Future Work

Though the result came as expected but there're still some improvements required for the prospective research:

1. The nano-particle deposition on the rod surface is a huge problem. Take a brave guess for the nano-fluid to be industrialized in reality, to provide effective solutions, we should look to substitute the surfactant that does not break down at higher temperatures. The is a possibility of using grapheme nano-particles that may not need any surfactact. A breakthrough in avoiding deposition of the particles may lead to a bright future for nano-fluids to perform as coolant.

2. The prediction of thermal conductivity of the nano-fluids is based on the experience equation of former researchers with different nanoparticles. Some equipment such as KD2 Pro will give a more precise thermal conductivity of nano-fluid.

REFERENCES

Shuichi Torii, 2009, "Turbulent Heat Transfer Behavior of Nano-fluid in a Circular Tube Heated under Constant Heat Flux", Hindawi Publishing Corporation Advances in Mechanical Engineering, Volume 2010, Article ID 917612, 7 pages

Jose R. Vazquez Penas, Jose M. Ortiz de Zarate and Mohamed Khayet, 2008, "Measurement of the thermal conductivity of nanofluids by the multicurrent hot-wire method", Journal of Applied Physics 104, 044314.

Yajie Ren, Huaqing Xie and An Cai, 2005, " Effective thermal conductivity of nanofluids containing spherical nanoparticles", Journal of Physics D: Applied Physics

J. P. STONE, C. T. EWING, and R. R. MILLER," Heat-Transfer Studies on Some Stable Organic Fluids in a Forced Convection loop"

Yimin Xuan & Qiang Li, 2009, "Investigation on Convective Heat Transfer and Flow Features of Nanofluids"

Liu, K. V., Choi, U. S., and Kasza, K. E., 1988, ‘‘Measurements of Pressure Drop and Heat Transfer in Turbulent Pipe Flows of Particulate Slurries,’’ report,Argonne National Laboratory ANL-88-15.

Steinke, M.E. and Kandlikar, S.G., 2005, “Single-Phase Liquid Heat Transfer in Microchannels” Proceedings of the International Conference on Microchannels and Minichannels, June 13-15, Toronto, Ontario, Canada, ICMM05-75114, ASME Publications.

Firth, R.J. and Meyer, L., 1983, “A comparison of the heat transfer and friction factor performance of four different types of artificially roughened surface”, Int. Journal of Mass and Heat Transfer, vol. 26, no. 2, pp. 175-183.

A.E. Bergles, A.R. Blumenkrantz, J. Taborek, 1974, “Performance evaluation criteria for enhanced heat transfer surfaces”, in: Proceedings of the Fourth International Heat Transfer Conference vol. 2, pp. 239-243.

Ryu, D.N., Choi, D.H., Patel, V.C., 2007, “Analysis of turbulent flow in channels roughened by two-dimensional ribs and three-dimensional blocks” Part I: Resistance. International Journal of Heat and Fluid Flow 28, 1098-1111.

Han, J.C., Park, J.S., and Lei, C.K., 1985, "Heat transfer in channels with turbulence promoters", *ASME Journal of Engineering for gas Turbine and Power,* Vol. 107, pp.628-635.

D. Ryu, D. Choi, V. Patel, 2007, "Analysis of turbulent flow in channels roughened by 1321 two-dimensional ribs and three-dimensional blocks": part II: heat transfer, Int. 1322 J. Heat Fluid Flow 28, pp. 1112–1124.

Han, J.C., 1984, "Heat transfer and Friction in channels with two opposite rib-roughened walls turbulators", *ASME Journal of Engineering for gas Turbine and Power,* Vol. 106, May, pp.774-781.

Han, J.C., Huang, J.J., Lee, C.P., 1993, "Augmented Heat transfer in square channels with wedge-shaped and delta-shaped Turbulence promoters", *Enhanced Heat Transfer,* Vol. 1, pp.37-52.

Xiao-wei Li, Ji-an Meng, Zhi-xin Li, 2011, "Roughness enhanced mechanism for turbulent convective heat transfer, International Journal of Heat and Mass Transfer", Volume 54, Issues 9–10, April, Pages 1775-1781.

A. Lanjewar, J.L. Bhagoria, R.M. Sarviya, 2011, "Experimental study of augmented heat transfer and friction in solar air heater with different orientations of W-Rib roughness", Experimental Thermal and Fluid Science, Volume 35, Issue 6, September, Pages 986-995.

Singh, S., Chander, S., Saini, J. S., 2011, “Heat transfer and friction factor correlations of solar air heater ducts artificially roughened with discrete V-down ribs”, Energy, Volume 36, Issue 8 , 5053–5064

A. Bejan, 2004, "Convection Heat Transfer", 3rd ed. Wiley, Hoboken, NJ.

A. Bejan, 2006, “Advanced Engineering Thermodynamics”, 3rd ed. Wiley, Hoboken, NJ.

Hugh W. Coleman and W. Glenn Steele Jr. 2009, "Experimentation, Validation, and Uncertainty Analysis for Engineers", Third Edition

Ralph L. Webb, Nae-Hyun Kim, 2005, "Principles of Enhanced Heat Transfer", Taylor & Francis.

Focke, W. W., Zachariades, J., and Olivier, I., 1985, "The Effect of the Corrugation Inclination Angle on the Thermohydraulic Performance of Plate Heat Exchangers" Int. J. Heat Mass Transfer, Vol. 28, pp. 1469-1479.

Stasiek, J., Collins, M. W., Ciofalo, M., and Chew, P. E., 1996, “Investigation of Flow and Heat Transfer in Corrugated Passages -- I. Experimental Results,” Int. J. Heat Mass Trans., Vol. 39, pp. 149-164.

R.J. Firth, L. Meyer, 1983, “A comparison of the heat transfer and friction factor performance of four different types of artificially roughened surface”, International Journal of Heat and Mass Transfer, Volume 26, Issue 2, February, Pages 175-183.

R. J. Firth, 1982, "An interpretation of the KfK heat transfer data for three dimensional roughness", Gas cooled reactors today. Volume 3, pp. 205-210.

L. Meyer, 1982, “Thermo-hydraulic characteristics of single rods with three-dimensional roughness”, International Journal of Heat and Mass Transfer, Volume 25, Issue 7, July, Pages 1043-1058.

Groehn, H. G., and Scholz, F., 1976, “Heat Transfer and Pressure Drop of In-Line Tube Banks with Artificial Roughness,” in Heat Mass Transfer Sourcebook: Fifth All-Union Conf., Minsk, Scripta Pub. Co., Washington, DC, pp. 21-24.